Polymer 309 (2024) 127453

Contents lists available at ScienceDirect

Polymer

journal homepage: www.elsevier.com/locate/polymer

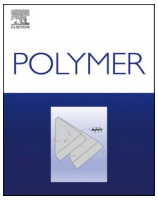

Surface modification strategies for improved cellulose nanocrystal integration in 3D-Printed bio-based acrylate matrix

Beate Beatrise Bruvere, Maksims Jurinovs, Oskars Platnieks *, Anda Barkane, Sergejs Gaidukovs **

Institute of Chemistry and Chemical Technology, Faculty of Natural Sciences and Technology, Riga Technical University, P. Valdena Str. 3, LV-1048, Riga, Latvia

ARTICLE INFO

Keywords:
UV-Curing
Photopolymerization
Nanocomposite
Nanocellulose functionalization
Acrylated epoxidized soybean oil

ABSTRACT

The current application of renewable resources in vat photopolymerization (VP) 3D printing is rather limited, emphasizing the importance of incorporating bio-based materials into additive manufacturing (AM). In this study, VP 3D printing technology was applied to create composites (derived from soybean oil-based resin) reinforced with cellulose nanocrystals (CNC). Two distinct modifications for CNC, i.e., the acrylation and functionalization with methyl methacrylate, were selected to achieve strong bonding with the UV-curable acrylate matrix. With the use of 0.1 wt% of modified CNC, the resins retain remarkable performance and support the creation of high-resolution prints. The successful integration of modified CNC showed significant improvements in tensile and flexural properties, e.g., elongation at break increased by 75 % and 295 %, respectively. The addition of modified CNC fillers also increased tensile strength by 147 % and flexural strength by 121 %. Fourier-transformation infrared (FTIR) spectroscopy and dynamic mechanical analysis (DMA) testified to the enhanced interface between filler and matrix. The morphological features and print quality were examined with microscopic analysis, UV-VIS spectroscopy, and colorimetry. The resin showed exceptional printing resolution, characteristic of VP printing, and yielded double bond conversion rates greater than 70 %. The findings presented here indicate that the addition of 0.1 wt% of modified CNC to bio-based resins results in an exceptional increase in the mechanical performance and dimensional stability of printed materials.

1. Introduction

Acrylic resin-based polymer systems derived from bio-based resources mark a pivotal shift towards sustainability in materials science, offering versatile alternatives to conventional petroleum-based polymers [1]. These bio-based systems find diverse applications across industries, including 3D printing and advanced coatings, showcasing their adaptability and potential [2]. Notably, bio-based acrylate photopolymer resins facilitate the production of complex prototypes via 3D printing, with a typical bio-based carbon content ranging from about 30 to 80 %, maintaining comparable mechanical and thermal properties to petroleum-based resins [3,4]. Furthermore, innovations in bio-based acrylic polymers and elastomers through controlled radical polymerization highlight these sustainable materials' broad applicability and performance [5]. Renewable alternatives derived from vegetable and plant oils further exemplify the feasibility of replacing conventional materials in various applications [6,7]. Collectively, these advancements underscore the significant strides in creating sustainable, high-performance materials that align with environmental goals and open new avenues in material science and engineering.

Cellulose nanocrystals (CNCs) stand out as a renewable, sustainable additive poised to revolutionize the properties of polymer resins, notably in photocurable systems, through their exceptional mechanical strength and low density (around 1.5–1.6 g/cm^3) [8]. In contrast, glass fibers have a 2.5 g/cm^3 density, carbon fibers range from 1.75 to 2.0 g/cm^3, and basalt fibers are around 2.7 g/cm^3. Originating from diverse cellulose sources via acid hydrolysis, CNCs offer notable enhancements in polymer matrices' mechanical, thermal, and barrier capabilities [8,9]. Their integration into photocurable resins has been particularly transformative, bolstering mechanical performance and infusing beneficial features such as tunable hydrophilicity and increased adhesion [10]. Despite numerous advantages, cellulose nanofillers are still prone to

* Corresponding author.
** Corresponding author.
E-mail addresses: Oskars.Platnieks_1@rtu.lv (O. Platnieks), Sergejs.Gaidukovs@rtu.lv (S. Gaidukovs).

https://doi.org/10.1016/j.polymer.2024.127453
Received 18 April 2024; Received in revised form 15 July 2024; Accepted 31 July 2024
Available online 2 August 2024
0032-3861/© 2024 The Authors. Published by Elsevier Ltd. This is an open access article under the CC BY license (http://creativecommons.org/licenses/by/4.0/).

agglomeration due to their high hydrophilicity, especially in oleophilic resin (matrix) [9]. Functionalized CNCs present a compelling approach to enhancing polymer composites' mechanical properties due to improved interfacial compatibility.

Dogan-Guner et al. prepared surface-grafted CNCs with isocyanatoethyl methacrylate and dispersed them in an acrylic polymer matrix [11]. The authors reported 100 % improvement in the tensile strength and about 53 % enhancement in the hardness of the acrylic matrix with 6 wt% loading, while unmodified CNCs did not increase properties. Ali et al. modified CNC with 2-carboxyethyl acrylate and dispersed them in epoxy resin system [12]. Loadings from 1 to 3 wt% of modified CNCs improved mechanical, adhesive, and thermal properties. Auclair et al. demonstrated that the addition of 1–2 wt% of acrylated CNC to acrylated epoxidized soybean oil (AESO)-based resin saw up to a 45 % improvement in elastic modulus and up to a 4-fold improvement in hardness [13]. Thus, the literature indicates that nanocellulose is compatible with acrylated vegetable oils and epoxy-based systems. In addition, the chemically modified nanocellulose shows superior properties to its non-modified counterparts.

Vegetable oil-based resins are hydrophobic, while bio-based nanocellulose fillers clearly favor a hydrophobic matrix. To overcome this challenge, a suitable modification method must be selected. We have opted for the acrylation of CNC and functionalization with methyl methacrylate as two distinct methods that could provide strong chemical bonding with an AESO-based matrix. To take full advantage of the nanofiller and show a significant impact that can be achieved, only 0.1 wt% of CNC is added to the resin. Lastly, compatibility with vat photopolymerization is demonstrated as all samples have been 3D printed from bio-based resins, achieving excellent resolution with a layer height of 0.05 mm.

2. Experimental

2.1. Materials

Acrylated epoxidized soybean oil (AESO) (contains 3500–4500 ppm monomethyl ether hydroquinone as an inhibitor, viscosity 18,000–32,000 cps.); reactive diluents: trimethylolpropane triacrylate (TMPTA) (purity of >70.00 %, contains 500–750 ppm monomethyl ether hydroquinone as inhibitor) and 1,6-hexanediol diacrylate-technical grade (HDDA) (purity 77.5 %); photoinitiator (PI): diphenyl (2,4,6-trimethyl-benzoyl) phosphine oxide (TPO); high purity (≥99.0 %) chemicals – acetone, ethanol, methyl methacrylate (MMA), ammonium cerium IV nitrate (CAN), N,N-dimethylacetamide (DMAc), acrylic chloride (AC), hydrochloric acid (HCl), and lithium chloride (LiCl) were purchased from Sigma-Aldrich. All received chemicals were used as is, except in instances where specific processing is stated. Cellulose nanocrystals (CNC) were obtained by processing *Santhica 27* variety hemp stalks.

2.2. Nanocellulose preparation

The processing of hemp stalks involved a sequential two-step milling operation. Initially, the stalks were subjected to coarse grinding using a Retsch SM300 cutting mill, outfitted with 4.00 mm and 0.25 mm sieves for consecutive stages. This was succeeded by a finer grinding phase in a Retsch ZM200 mill equipped with a 0.12 mm sieve. Hemp powder was then treated with a 10 % aqueous NaOH solution, following a 1:8 mass ratio, and stirred at 80 °C for 3 h. The alkaline treatment was refreshed with a new NaOH solution and left to stand overnight at room temperature (20 °C). The resultant pulp was filtered and rinsed with deionized water to achieve a neutral pH. The pulp was then subjected to an acid treatment using a 20 % aqueous HCl solution at a 1:8 ratio based on the dry weight of the cellulose and heated at 80 °C for 2 h. After acid processing, the cellulose was filtered and rinsed until neutral pH was reached. The cellulose was re-suspended in water at a 1 wt% concentration and processed through an LM 20 Microfluidizer (USA) with an H210Z chamber (200 μm) at 30,000 psi. This procedure, entailing five passes through the microfluidizer, yielded CNC.

2.3. CNC acrylation

The acrylation of cellulose nanocrystals (CNC) was performed as described by Qian et al. [14]. Initially, a suspension was prepared by dispersing 1.25 g of CNC in 24 mL of anhydrous DMAc at 120 °C for 1 h. Subsequently, 3 g of LiCl was incorporated into the mixture, which was then stirred for 30 min. Upon cooling to room temperature, the mixture was allowed to stabilize overnight. 3.5 g of acryloyl chloride (AC) was added to the resultant homogeneous solution while the solution was cooled in an ice/water bath. The solution temperature was then raised to 50 °C and stirred continuously for 3 h. After cooling back to room temperature, the polymer was separated by precipitating it in ethanol. Further purification was achieved by dissolving the precipitate in 60 mL of acetone and re-precipitating it in ethanol, forming a white powder identified as acrylated CNC (ACNC). The ACNC was immediately transferred to a small amount of acetone.

2.4. CNC functionalization with methyl methacrylate

Spinella S. et al. detailed the modification of CNC with MMA in their work [15]. Briefly, an aqueous CNC suspension (2 g in 200 mL) was subjected to sonication for 10 min at 25 °C, followed by degassing through nitrogen bubbling for 30 min at 35 °C. The pH of the suspension was adjusted to 1 using nitric acid (HNO_3), after which CAN (1 g) and MMA (4 g) were introduced. The reaction proceeded under a nitrogen atmosphere for 2 h at 35 °C. After the reaction, the product was isolated through centrifugation at 10,000 rpm for 30 min, repeated five times, until a neutral pH was attained. For purification, acetone was utilized as the solvent, and the product underwent Soxhlet extraction for 24 h, yielding CNC grafted with polymethyl methacrylate (PMMA), abbreviated as MACNC). The MACNC was stored in a small amount of acetone.

2.5. Preparation of the resins

The process began by mixing monomers with a dissolved photoinitiator, TPO, in acetone, followed by adding AESO. This mixture was subjected to mechanical stirring for 1 h. The resin's composition was fixed to be 65/30/5 wt%, consisting of AESO, HDDA, and TMPTA. A photoinitiator to resin weight ratio of 3:100 was employed to achieve a photoactive mixture. Subsequently, a dispersion of cellulose nanocrystals (CNC, ACNC, and MACNC) in acetone was incorporated into the resin using a high-shear mixer for 5 min at 9000 rpm. To remove entrapped air and residual acetone, the mixture was placed in a vacuum chamber maintained at 1000 mbar for 2 h at room temperature (20 °C). The prepared resins were stored away from light to prevent premature curing. The concentration of the filler within the resin was fixed at a constant 0.1 wt%. After being used for sample printing, it was noted that the resin exhibited no sedimentation for the observed duration (one month).

2.6. 3D printing of the samples

Samples were fabricated using an Original Prusa SL1 3D printer, equipped with a 5.5-inch LCD and a 25 W LED emitting at 405 nm UV wavelength. These samples were designed for mechanical testing, adhering to ISO-178 for flexural tests with dimensions of 80 × 10 × 4 mm and ISO-527 1BA for tensile tests measuring 75 × 10 × 2 mm. The print settings included a layer height of 0.05 mm, with the first 10 layers exposed for 35 s to ensure adhesion to the platform and subsequent layers exposed for 15 s. Post-printing, the samples were cleaned with isopropanol, dried for 5 min, and then post-cured for 3 min in a Prusa Curing and Washing Machine at 405 nm UV light and 20 °C. The

abbreviations of four printed compositions and respective fillers are shown in Table 1.

2.7. Fourier-Transform infrared spectroscopy (FTIR)

FTIR configured in attenuated total reflection (ATR) sampling technique was performed on a Nicolet 6700 spectrometer at a resolution of 4 cm^{-1} from 400 to 4000 cm^{-1}. FTIR was configured to measure and display the average spectrum of sixteen scans.

Double bond conversion rate % (DBC%) was calculated using the equation (1):

$$DBC\% = \left(1 - \left(\frac{A_t}{A_{ra}}\right) \Big/ \left(\frac{A_0}{A_{rb}}\right)\right) \times 100\%, \quad (1)$$

where A_{rb} and A_{ra} are the absorption intensities of the peak at 1733 cm^{-1} before and after UV-crosslinking; A_0 and A_t are the absorption intensities of the 810 cm^{-1} peak before and after UV-crosslinking. The peak selection is based on resin curing analysis discussed in depth in the previous work [16].

The theoretical FTIR spectra were calculated using equation (2):

$$A_{Xf} = X \times A_f + (1 - X)A_{pol} \quad (2)$$

where A_f and A_{pol} are the absorbances (%) for components in the composition spectra, cellulose nanocrystal component (f), and polymer matrix (p), respectively. X = wt% of a cellulose nanocrystal component in a specific composition.

2.8. Atomic force microscopy (AFM)

AFM was performed on Smena, NT-MDT with HA_NC (ETALON) tip in semi-contact mode to characterize CNC particles and 3D printed sample fracture surfaces. CNC dispersion of 0.005 wt% was dropped on the Si glass substrate and dried overnight at 50 °C; the diameter was measured based on the height in topography, with corrections applied to account for the apparent length caused by the used tip. For fracture surface characterization, samples were broken in ambient conditions.

2.9. Contact angle

The contact angle was measured with a Theta Lite optical tensiometer to test the change in hydrophilicity. CNC filler film was formed on a glass substrate and the suspension was dried overnight at 40 °C using vacuum oven. The contact angle was determined at the fifth second at room temperature (20 °C). Modified nanocellulose was dropped on a glass substrate and dried.

2.10. Thermogravimetric analysis (TGA)

TGA was performed on a Mettler Toledo TG50 instrument. Samples weighing approximately 10 mg were heated in a nitrogen (N_2) environment at 10 °C/min from 25 to 700 °C. Material thermal stability was evaluated from the weight-loss heating curves.

2.11. Optical microscopy

Optical microscopy measurements were performed on a Leica 301–371.011 DMRBE optical microscope (Germany) with 200 × magnification, and Leica application suite software was used to obtain images of the top and side surfaces of the 3D printed samples.

Table 1
3D-printed sample abbreviations.

Printed sample	Filler	Filler loading (wt%)
p0%	–	–
pCNC	Cellulose nanocrystals (CNC)	0.1
pACNC	Acrylated CNC (ACNC)	
pMACNC	MMA functionalized CNC (MACNC)	

2.12. Ultraviolet–visible spectroscopy (UV-VIS)

UV-VIS spectra were measured using a SolidSpec3700 UV-VIS-NIR Shimadzu spectrophotometer in the wavelength range from 240 to 700 nm in reflectance and transmittance modes. The 500 nm spectral line was chosen to compare the transmittance data for samples with a thickness of 4.0 mm.

2.13. Density

The hydrostatic weighing method was performed on a Sartorius MC1 analytical balance (Germany, Burladingen) to determine the density of the printed samples. Samples of approximately 45 mg were prepared, and then 10 parallel measurements were carried out in air and ethanol. Scale accuracy was 0.00001 g.

The sample density was calculated according to equation (3):

$$\rho = \frac{m_a \times (\rho_{C_2H_5OH} - 0.0012)}{0.99983 \times (m_a - m_{C_2H_5OH})} + 0.0012 \quad (3)$$

where ρ is the density of the sample, m_a is the mass of the sample in air, ρ_{C2H5OH} is the density of the used ethanol, and m_{C2H5OH} is the mass of the sample in ethanol.

2.14. Sol fraction

A Soxhlet extraction setup was used to determine the part of the polymer that is not cross-linked and can be dissolved. 10 parallel samples (4 × 4 × 2 mm) of each printed composition were 3D printed. Sol fraction analysis was performed in acetone for 72 h.

2.15. Colorimetry

Color changes were evaluated using the Ci7600 Sphere Benchtop Spectrophotometer (x-rite Pantone, Michigan, USA). Three parallel measurements were done with a total transmittance aperture of 6 mm, a wavelength range of 360–750 nm, a photometric resolution of 0.01 %, and white paper to avoid color darkening from the black background due to the transparency of the samples. The ΔE^*_{ab} values are calculated by the manufacturer's software and indicate the quantitative color changes of the samples in reference to the sample with no CNC (p0%).

2.16. Mechanical testing

According to EN ISO 527-1BA standard, tensile tests were conducted on dog bone shaped samples that were 3D printed and had dimensions of 30 × 5 × 2 mm in the central section. Using a Tinius Olsen 25ST universal testing machine equipped with a 5 kN S-type load cell, the initial region was tested at 1 mm/min for the tensile modulus, while afterward, 5 mm/min speed was used. In accordance with EN ISO-178, three-point flexural tests were conducted on rectangular samples that were 3D printed and had dimensions of 80 × 10 × 4 mm. Using a Tinius Olsen 25ST universal testing machine equipped with a 5 kN S-type load cell, the testing speeds were 1 mm/min for flexural modulus, while afterward 5 mm/min speed was used. Prepared specimens were stored in a sealed bag at room temperature (20 °C). Average values were obtained from the testing of 5 specimens. All tests were performed two days after the printing of the specimens in ambient conditions (20 °C, 40 RH).

2.17. Dynamic mechanical analysis (DMA)

DMA was performed on a Mettler Toledo SDTA861e analyzer in the range from −70 to 100 °C, with a heating rate of 3 °C/min, a frequency

of 1 Hz, a displacement of 20 μm, and a force of 10 N. 3D printed samples with 80 × 10 × 4 mm dimensions were used. Dual cantilever deformation mode was used.

To determine the molecular weight between crosslinks M_c and crosslinking density N were calculated using equations (4) and (5):

$$M_c = \frac{3\rho RT}{E'} \quad (4)$$

$$N = \frac{\rho}{M_c} \quad (5)$$

where ρ is the density of the printed sample, E′ is the storage modulus at 95 °C, T is the temperature at which E′ is acquired and R is the gas constant.

3. Results and discussion

3.1. CNC modification analysis

The FTIR spectral analysis of both unmodified and chemically modified CNC in Fig. 1 allows to evaluate the functionalization of the fillers. A broad absorption band spanning from 3000 to 3600 cm^{-1}, highlighted in grey in Fig. 1, ascribes to the stretching vibrations of the hydroxyl (OH) groups inherent to cellulose [17]. A distinct absorption peak at 1726 cm^{-1}, marked in yellow in Fig. 1, indicates the stretching vibrations of carbonyl groups within an ester linkage [14,15,18]. Simultaneously, a pronounced decrease of the OH peak with the increase of the carbonyl group peak indicates the successful functionalization of the fillers. The spectra of ACNC revealed new notable absorption bands at 810 and 1634 cm^{-1}, characteristic of the vibrations associated with vinyl bonds in the grafted acrylic moieties [14,18]. The CNC modified with methyl methacrylate (MACNC) exhibits only a minor peak at 810 cm^{-1}, consistent with the anticipated self-polymerization of MMA. Furthermore, CNC displays significant absorption in the 1000–1100 cm^{-1} range, correlating with C–O stretching vibrations [17]. All fillers exhibit C–O–C stretching vibrations at 1160 cm^{-1} [19]. In contrast, CNC that has been surface-modified does not exhibit a significant peak at 895 cm^{-1}, which is typically attributed to the β-linkage found in cellulose [20].

3.2. CNC filler morphology, surface, and thermal stability

The AFM images in Fig. 2a and **c** reveal the presence of nanocellulose filler particles. AFM analysis indicates that the functionalization process led to a marginal increase in the size of the particles of the MACNC. The dimensions obtained and their statistical variations are detailed in Table 2. For ACNC particles, measurement was impossible due to the functionalized ACNC's instability in its dry form. Nanocellulose particles exhibit a propensity to agglomerate, while specifically for ACNCs, they also undergo polymerization in the absence of a solvent. This phenomenon results in a discernible coating of ACNC, as illustrated in Fig. 2b.

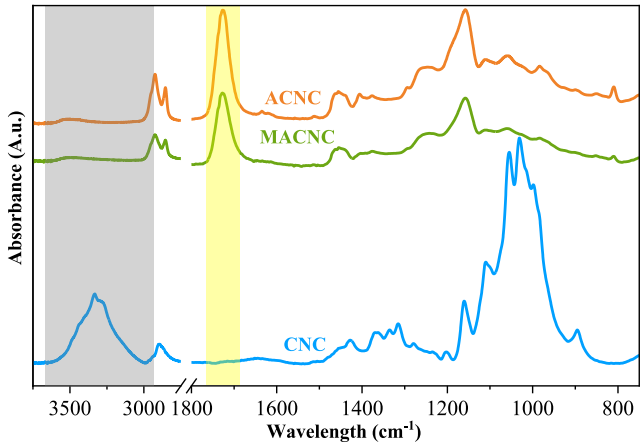

Fig. 1. FTIR spectra of nanocellulose fillers.

Surface wetting experiments were conducted to assess the potential reduction in the hydrophilicity of nanocellulose surfaces. Films of nanocellulose were created through suspension casting and subsequently dried. The contact angles and their corresponding statistical values are displayed in Fig. S1 and Table 2, respectively. Upon contact with the CNC, the water droplet immediately spreads across the surface; therefore, a contact angle of 0° is presented. For the ACNC and the MACNC, the contact angles were measured at 61° and 80°, respectively. Since each glucose unit in nanocellulose possesses three hydroxyl groups, contributing to its inherent strong hydrophilicity, the recorded contact angle values reflect successful chemical modifications. These modifications suggest a partial replacement of the hydroxyl groups, altering the surface characteristics of the nanocellulose. We also measured the contact angle of resin on CNC films and saw a slight improvement in resin being able to wet the modified CNC better than a neat CNC.

The thermal stability of nanocellulose fillers, with the derivative weight loss and weight loss curves, is presented in Fig. 2d and **e**, respectively. The maximum degradation temperature (T_{max}) and char yield are shown in Table 2. The distinct differences in thermal stability serve as indirect evidence of the chemical modification of the CNC surface. The analysis unequivocally demonstrates that CNC exhibits superior thermal stability compared to their acrylated (ACNC) and methacrylated (MACNC) counterparts. Notably, MACNC displayed the highest T_{max} at 378 °C, yet it showed continuous weight loss beginning from 120 °C. The elevated T_{max} observed for MACNC is likely due to the presence of thermally stable PMMA chains, which range in T_{max} from 350 to 400 °C and shield the cellulose from thermal degradation [21,22]. The weight loss for ACNC starts around 180 °C and is more pronounced above 200 °C, ultimately resulting in the lowest T_{max} among the samples. The observed differences in char yield are mainly due to char formation on the surface, which restricts complete degradation at elevated temperatures.

3.3. Characterization of filler/matrix interface in the 3D-printed samples

The morphological attributes of 3D-printed rectangular samples were evaluated using AFM (for examining fracture surfaces), optical microscopy (for analyzing top and side surfaces), and colorimetry. AFM analysis was conducted in semi-contact mode, producing 3D representations depicted in Fig. 3a. A visual inspection of the AFM fracture surface does not reveal visible CNC particles or their agglomerates. The samples pCNC and pACNC exhibit a rougher fracture surface texture compared to the smoother fractures of p0% and pMACNC. However, the overall scale shows that these differences are within the margin of error. AFM images indirectly suggest that effective dispersion of CNC and modified CNC within the polymer matrix has been achieved. The printing process's precision is evidenced in Fig. 3b and **c**, where the delineation of individual pixels (50 × 50 μm) on both the top and side surfaces of the rectangles is distinctly visible, demonstrating maintained printing accuracy of 50 × 50 μm. However, incorporating CNC reinforcement is slightly compromising the sample surface quality. Among the samples, MACNC exhibits a surface quality that most closely matches that of the p0% sample, with minimal defects on both the top and side views. The visible spots in the optical images on the surface of samples (with CNC fillers) are not CNC particle agglomerates but rather surface finish defects that remain after the post-processing step. This only occurs when the print is post-processed, and defects are only present on the surface.

Fig. 3d provides visual measurements of the color alterations attributed to the addition of CNC reinforcement, alongside quantifying these changes through the color difference factor (ΔE^*_{ab}). This metric

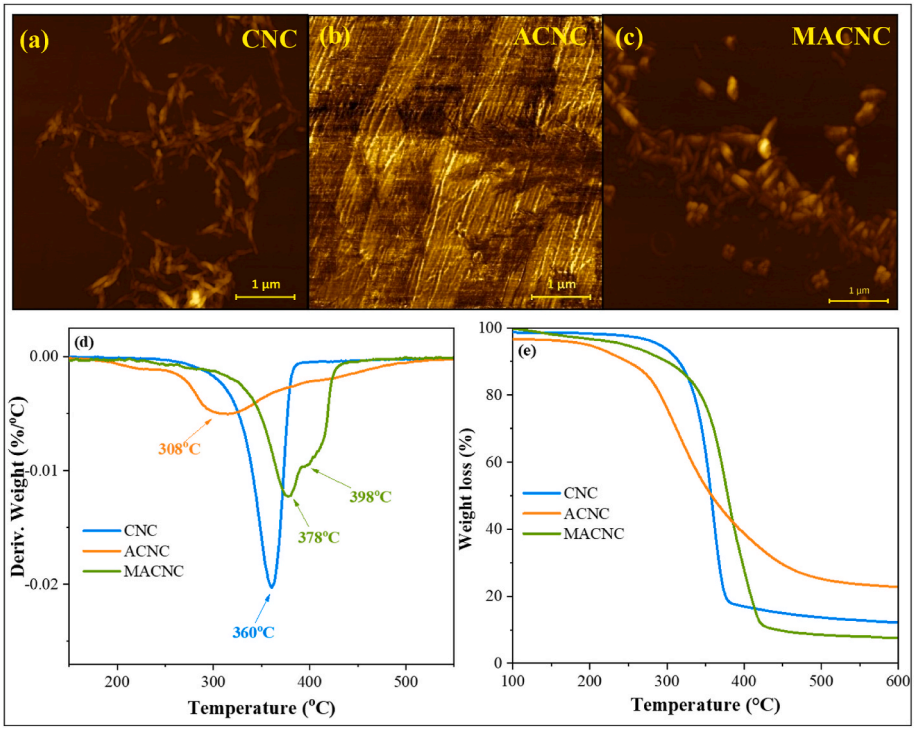

Fig. 2. AFM images of the CNC (a), ACNC (b) and MACNC (c). Thermal stability of the CNC fillers: derivative weight (d) and weight loss (e).

Table 2
Nanocellulose dimensions, wetting angle, and thermal parameters.

Sample	CNC	ACNC	MACNC
Diameter (nm)	33 ± 2	-	40 ± 5
Length (nm)	224 ± 74	-	232 ± 76
Contact angle (°) water	0	61 ± 3	80 ± 2
Contact angle (°) resin	26 ± 3	21 ± 2	23 ± 2
T_{max} (°C)	360	308	378
Char yield (%)	11	20	7

quantifies the deviation in color from the p0% sample, with the pCNC sample exhibiting the most pronounced change ($\Delta E^*_{ab} = 3.6$) and the pMACNC sample displaying the least ($\Delta E^*_{ab} = 2.0$). Despite these variations, the changes in ΔE^*_{ab} values are considered relatively minor. According to a study by Mokrzycki and Tatol, ΔE^*_{ab} value below 2 is perceptible only to the trained eye, a value between 3.5 and 5 signifies a noticeable difference, and a value above 5 suggests a discernible contrast in colors [23]. Conversely, the ViewSonic corporation homepage notes that in the realms of commercial reproduction, printing, and graphic design, an ΔE^*_{ab} value range of 3–6 is typically deemed acceptable [24]. As shown in Fig. 3e, UV-VIS spectroscopy was utilized to measure the light transmittance and reflectance. Commonly, composites incorporating nanoparticles exhibit reduced transmittance. This reduction is attributed to the scattering of visible light by the nanoparticles. The extent of light scattering by these particles is influenced by their size, composition, and the degree of refractive index matching between the particles and the surrounding matrix [25]. Incorporating neat CNC into the polymer matrix was observed to have a minimal effect on the material's transparency. pMACNC exhibited a slight improvement in transparency compared to pCNC, whereas pACNC experienced a significant decrease in transparency within the 430–600 nm range. Typically, changes in transparency are linked to the nanoparticle weight (volume) content. As observed with pCNC, the content does not significantly impact transparency, and all fillers display relatively good dispersion without visible agglomeration. Therefore, the changes observed for functionalized CNC can be attributed to alterations in surface chemistry and interactions with the matrix. ACNC is capable of forming covalent bonds with the matrix, resulting in strong interactions that could impact the matrix more than anticipated.

3.4. Macromolecular chain network and thermal stability of 3D printed samples

The focus on the C=O peak in FTIR spectroscopy provided insights into the hydrogen and other non-covalent bonding interactions between the filler and the polymer matrix (Fig. S2). The comprehensive FTIR spectra for the resins and printed samples are depicted in Fig. S3. Prior research indicates that the effect of hydrogen bonding on the matrix's C=O peak at 1727 cm^{-1} is characterized by a decrease in peak intensity and a shift in peak position [26]. These phenomena can be quantitatively assessed by calculating the intensity reduction using Lambert-Beer's equation, facilitating the prediction of theoretical FTIR spectra. Deviations from these theoretical predictions typically indicate hydrogen bonding or alternative non-covalent interactions with the CNC filler.

Two distinct behaviors were noted in the analysis of interactions between the polymer matrix and various cellulose fillers: a decrease in peak intensity for samples pCNC and pMACNC and a significant shift in the peak maximum for the pACNC. This discrepancy between the theoretical and measured spectra underscores the capacity of neat CNC to establish relatively strong intermolecular bonds with the matrix. The notably weaker intensity observed for pMACNC suggests that cellulose modified with MA fosters stronger bonds due to its reduced surface hydrophilicity. The unique behavior of pACNC might be attributed to the potential for forming covalent bonds with the matrix. The proposed mechanisms of covalent and hydrogen bonding between the matrix and CNC or modified CNCs are schematically illustrated in Fig. 4, explaining the complex interplay of molecular interactions that influence the material's properties. It should be noted that we focus our discussion on hydrogen bonding. Still, in the case of pMACNC, where grafted PMMA chains can form, other non-covalent bonding could provide an even stronger contribution to the interface formation.

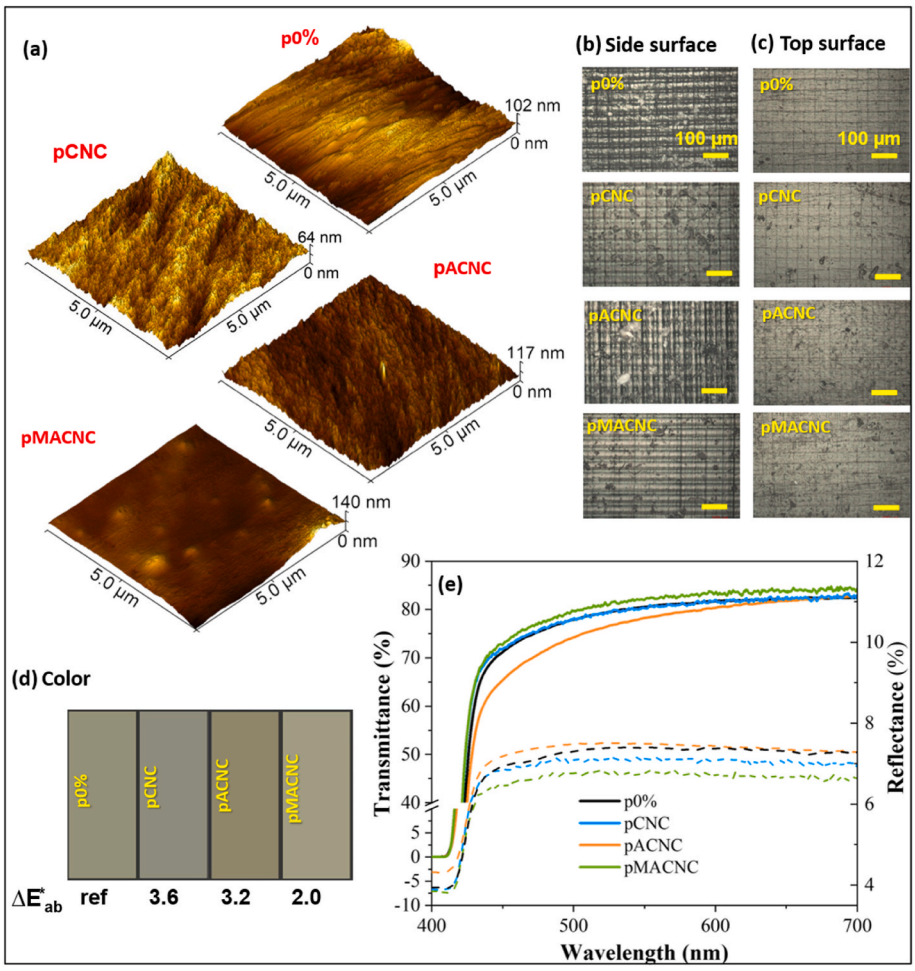

Fig. 3. AFM 3D images of fracture surface (a), optical microscopy images of samples side (b) and top (c) surfaces, colorimetry color images with color deviation ΔE^*_{ab} (d) and UV-VIS curves: transmittance (solid line) and reflectance (dashed line) for printed samples (e). (For interpretation of the references to color in this figure legend, the reader is referred to the Web version of this article.)

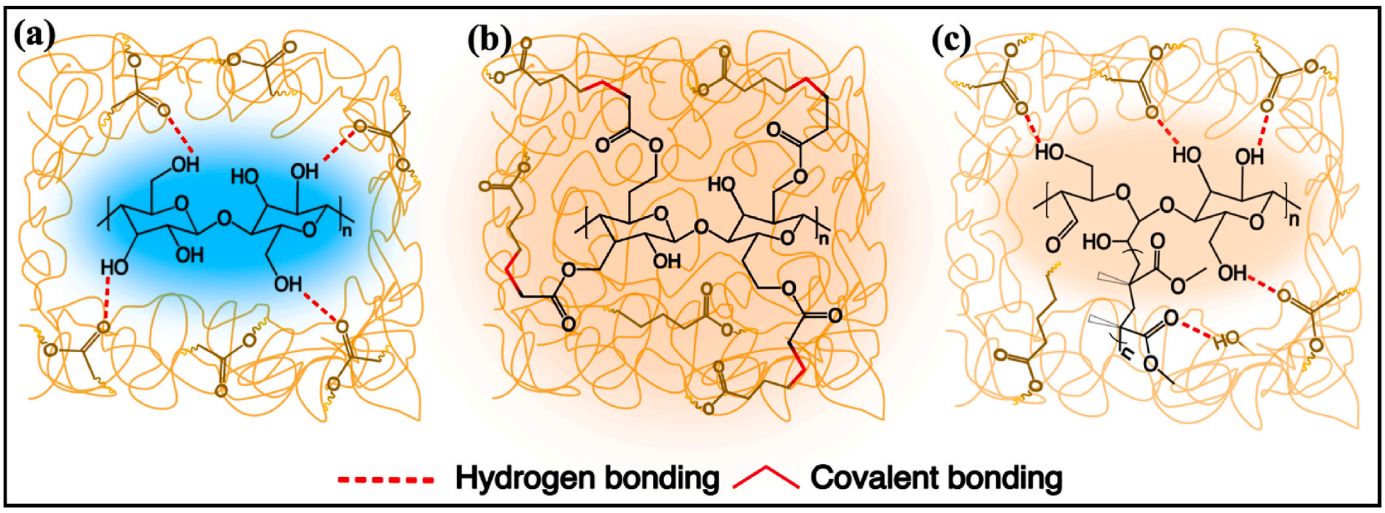

Fig. 4. Proposed filler-matrix interaction schematic representation for pCNC (a), pACNC (b) and pMACNC (c).

The efficacy of photo-crosslinked acrylate materials is intrinsically linked to the characteristics of the polymer network formed during the process. Parameters such as double bond conversion rates (DBC%), density, sol fraction, molecular weight between crosslinks (M_c), and crosslink density (N) have been selected and summarized in Table 3 to evaluate this. FTIR spectra, which facilitated the calculation of DBC% utilizing Equation (1), are illustrated in Fig. S3. The peak at 1733 cm^{-1}, attributed to AESO ester C=O vibrations, and the peak at 810 cm^{-1}, attributed to the double bond (C=C) vibrations of the resin components, were used for DBC% calculation. A comprehensive characterization of

Table 3
Structural characteristics of the 3D printed samples.

3D printed samples	p0%	pCNC	pACNC	pMACNC
DBC%, (%)	83	72	76	75
Sol fraction, (%)	3.7 ± 0.2	5.6 ± 0.8	5.5 ± 0.3	5.4 ± 0.6
N, (mmol/cm^3)	1.1	1.8	1.6	2.1
M_c, (g/mol)	1021	600	787	537
Density, (g/cm^3)	1.128 ± 0.001	1.125 ± 0.002	1.130 ± 0.003	1.126 ± 0.015

the FTIR peaks and the curing process is provided in our previous work [16]. The p0% achieves the highest DBC% at 83 % due to the absence of fillers. Meanwhile, printed samples with modified CNCs yielded an enhanced DBC% compared to pCNC. The CNC might impede radical and molecular mobility, obstructing the crosslinking reaction. The surface functionalization of cellulose may facilitate their incorporation into resin and matrix structures, potentially minimizing the restrictive effects during the network's formation. Moreover, a direct correlation was identified between the sol fraction data and the presence of fillers. The p0% sample showed the lowest sol fraction at 3.7 %, whereas composite samples exhibited higher sol fractions, ranging from 5.4 to 5.6 %. This variance further accentuates the influence of filler. The observed composite density values exhibited minimal deviation from those of the p0% sample, an outcome that aligns with expectations given the low filler loadings and the decreased DBC%.

Examining the macromolecular chain network and the interaction between fillers and the matrix can be done via calculations of crosslink density (N) and the molecular weight between crosslinks (M_c). These calculations are based on applying the theory of entropic rubber elasticity to the rubbery plateau modulus, as determined through DMA measurements [27]. This approach facilitates the enumeration of active cross-links within the system, encompassing chemical and physical varieties. The pMACNC sample exhibits the highest N value, suggesting it possesses the most significant aggregate of bonds among all the examined samples. This could be related to MA's ability to polymerize, resulting in polymethyl methacrylate grafted chains [15]. These could encompass CNC particles much more effectively and entangle with the matrix structure. Conversely, the pACNC sample is distinguished by having the lowest N value among the composite samples. This observation may be attributed to suboptimal bonding at elevated temperatures, a phenomenon that becomes evident upon analyzing the thermomechanical performance of the samples, as detailed in the subsequent discussion and illustrated in Fig. 6a.

The thermal stability of 3D-printed nanocomposite samples is presented in Fig. 5, which includes the weight loss curve alongside its derivative curves, illustrating the thermal decomposition characteristics of the samples. The polymer matrix provides thermal protection to the functionalized CNC, ascribed to the low filler loadings utilized in the composites. The primary peak in the derivative curves corresponds to the degradation of the acrylated AESO-based matrix [16]. The peak ranges from 420 °C to 423 °C, with the p0% sample exhibiting the highest maximum degradation temperature of 423 °C. The predominant weight loss for all samples occurs within the temperature range of 320–500 °C. The initial 5 wt% loss varies depending on the specific type of functionalized CNC employed, occurring at temperatures between 310 and 337 °C. This was attributed to changes in DBC%, as CNC only contributes to 0.1 wt%. Furthermore, the char yield percentage, indicative of the residual mass post-thermal degradation, is notably consistent across all printed samples, ranging between 3 and 4 %.

3.5. Thermomechanical performance and reinforcement efficiency

Polymer-based matrices demonstrate a pronounced dependence on the temperature, a characteristic related to the application temperature range. The glass transition is observable through a distinct shift from a

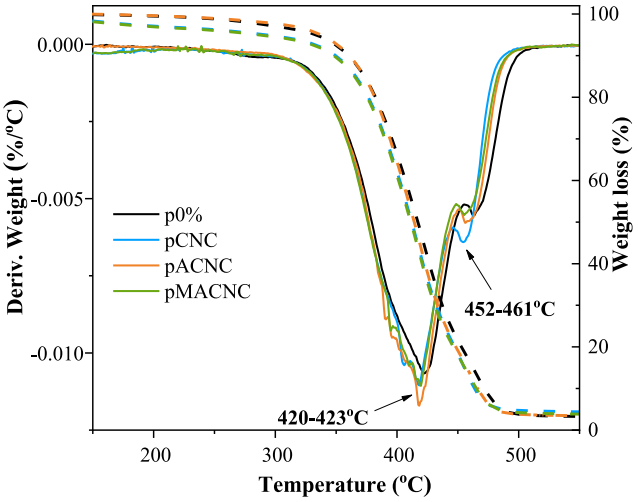

Fig. 5. Thermal stability of the 3D printed nanocomposite samples.

rigid, glassy state to a more flexible, viscoelastic state, accompanied by a sharp decrease in storage modulus (Fig. 6a). Such transitions are pivotal for understanding the mechanical properties of these materials under varying thermal conditions. In addition, the glass transition serves as a critical temperature region where the material undergoes significant changes in molecular mobility and relaxation processes. In a viscoelastic state, the filler (CNC) can affect the vegetable oil-based matrix and provide significant reinforcement. Our composites' glass transition temperature (T_g) matches the loss peak maxima (Fig. 6b) and is essential for assessing the compatibility between filler and matrix. This is further exemplified by the observed changes in T_g, which underscores the impact of intermolecular bonding and the mobility of polymer chains on the material's overall performance.

The impact of CNC reinforcement can also be seen from tanδ peaks (Fig. 6c). The decreased peak intensity shows that materials have become more rigid with increased stiffness, resulting from the loss to storage modulus value ratio shift. In addition, the tanδ peak saw a visible shift towards higher temperatures, with pCNC and pMACNC showing the splitting of a peak, appearing as a large shoulder to the main peak. This shift in tanδ curves is attributed to the restricted mobility of polymer chains, which is further amplified in the regions close to filler particles. It can be proposed that the composite structure now has distinct regions with higher crosslinking density (representing the formed maximum at around 65 °C), while more loosely connected regions form the shoulder part of the tanδ peak. pACNC forms a distinct case that does not follow the trend established by pCNC but instead resembles more p0% with a notably shifted peak maximum. This could be attributed to acrylated cellulose integrating into the matrix more seamlessly, owning to surface functionality that can participate in the crosslinking reaction.

The reinforcement effect of CNC is illustrated in Fig. 6d, demonstrating the stress transfer from the matrix to the filler. The depicted curves quantify this interaction by illustrating the composite's storage modulus ratio relative to the matrices. Notably, above 10 °C (post-glass transition temperature), a marked divergence in mechanical properties between the composite materials and the matrix is observed. The reinforcement effect manifests as an increasing divergence from the matrix's mechanical properties, with a progressive amplification observed, culminating in a 3.4-fold difference. This maximal divergence is attained in the vicinity of 70 °C. Comparative analysis among different composite formulations reveals that the MACNC filler performs better, surpassing CNC and ACNC in efficacy. The comparatively subdued performance of pACNC can be explained by its unique bonding structure, which, in

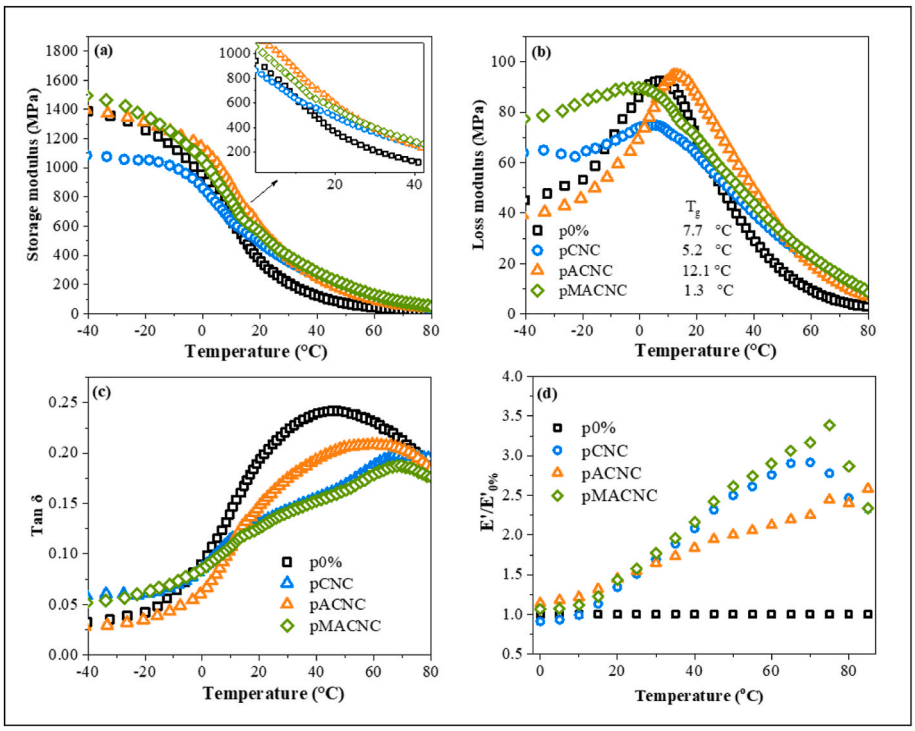

Fig. 6. Storage modulus (a), loss modulus (b), Tan δ (c), and ratio between composites and matrix storage modulus values (d).

contrast to other composites, does not exhibit a significant reduction in reinforcement beyond 70 °C.

3.6. Mechanical properties

To further explore mechanical performance, tensile and flexural tests were performed, and the results are summarized in Fig. 7. From the start, composites show superior performance to p0% in all but flexural modulus values. Detailed examination of Fig. 7a reveals that the elongation at break attained during tensile testing is high across all composite variants, with a notably higher increase observed in the pMACNC, while pCNC and pACNC are within the statistical error margins. pMACNC composite compared to p0% shows an impressive 75 % and 295 % enhancement in elongation at break values for tensile and flexural tests (Fig. 7b), respectively. Tensile strength revealed similarly impressive results, reaching a 147 % increase in tensile strength and 121 % in flexural strength when comparing modified CNCs to p0%. In this case, pACNC showed slightly higher performance in flexural strength, while pMACNC in the tensile strength. Flexural modulus values showed impressive performance for p0%, which was only slightly exceeded by pACNC. pACNC showed the best modulus values overall, with a notable 76 % increase in tensile modulus compared to p0%.

The high modulus values observed for pACNC (Fig. 7c) coincide with the higher glass transition temperature, which is relatively close to room temperature for pACNC. At the same time, pMACNC benefited from its lower glass transition temperature, which is reflected in higher elongation values. Tensile and flexural strength values are exceptionally high across all composites, indicating that not just ACNC and MACNC but even CNC poses good compatibility with the matrix. This illustrates that CNC fillers add extra dimensional stability, owning to increased intermolecular bonding and reinforcing effects. Notable is an effect on the enhanced elongation at break values, indicating that composites can distribute stress much more evenly. Therefore, sample failure is less based on the structural defects introduced during the printing and subsequent UV-curing.

We compared the tensile test results of our samples with those in existing scientific literature, as shown in Fig. 8, which contains the Ashby plot. For comparison, three AESO- and one epoxy-based system with modified CNC fillers were selected. It should be noted that the preparation method, cellulose source, and varying sizes of CNC play significant roles in their interactions with the matrix and the reinforcement provided. For example, hydrochloric acid hydrolysis results in CNC with little surface charge, while sulfuric acid esterifies surface hydroxyl groups into charged sulfate groups to produce more stable aqueous suspensions [30]. This difference can impact the CNC modification process. Composites with similar matrix properties were chosen, while two (3 and 4) used a 3D printing approach for sample preparation. Auclair et al. (2) presented findings indicating that integrating 1 to 2 wt % of acrylated CNC into an AESO-based resin not only resulted in a significant increase in both the elastic modulus, by up to 45 %, and hardness, by up to a factor of four, but also led to a modest increase in tensile strength alongside a slight reduction in elongation at break values [13]. Among the tested loadings of 1 and 2 wt%, it was observed that the performance was enhanced more at the lower loading. Unfortunately, the authors did not study composites with unmodified CNC. Liu et al. (3) prepared 3D-printing resin from AESO and ethyl cellulose modified with methyl acrylate groups, which the authors referred to as modified ethyl cellulose macromonomer (ECM) [28]. The authors reported that a higher modified cellulose content yielded higher mechanical properties. Notable was that the authors reported a 6-fold increase in modulus while achieving similar or slightly higher elongation values compared to neat AESO (23 %). Compared to this work, the authors used a syringe-based 3D printer, which significantly reduced the printing resolution. Wang et al. (4) used methacrylic resin and MA-grafted CNC as reinforcement with loadings from 0.1 to 1 wt% for VP 3D printing [29]. The mechanical analysis was compared to a 0.5 wt % loaded composite with unmodified CNC. All modified CNC composites exceeded the performance of unmodified CNC composites, achieving a 46 % increase in tensile strength and a 32 % increase in modulus at 0.5 wt% modified CNC loading. The 0.5 MA-grafted CNC was the optimal loading reported, with the exception of 0.1 wt% showing the highest elongation values. Ali et al. (5) modified cellulose nanocrystals (CNCs) with 2-carboxyethyl acrylate and dispersed them in an epoxy resin system [12]. Loadings 1 and 3 wt% of modified CNCs were

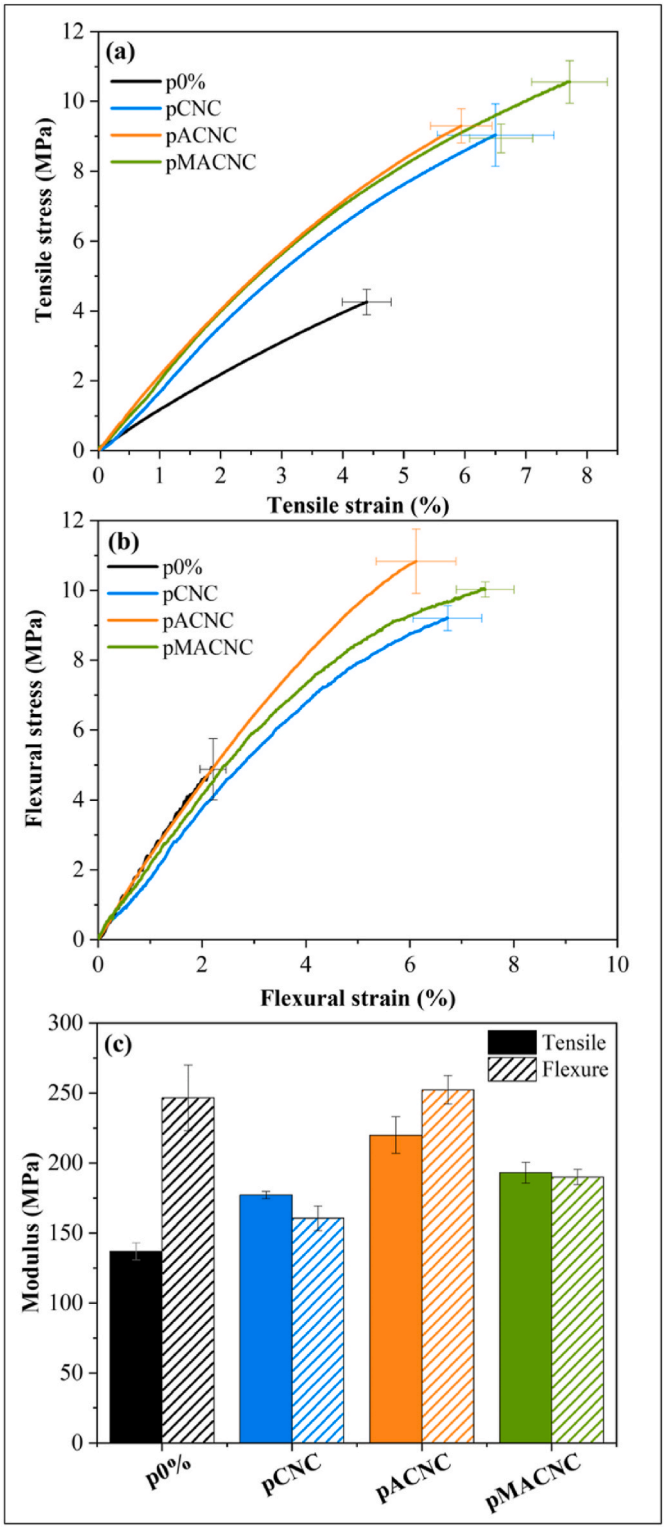

Fig. 7. Mechanical properties of the 3D printed samples – tensile stress vs strain curves (a), flexural stress vs strain curves (b), and modulus (c).

compared to their unmodified counterparts with loadings from 1 to 5 wt %. The authors showed that 1 wt% loading did not present notable differences, but in the case of 3 wt% modified CNC loading, the best overall results were achieved when compared between all composite formulations. It can be seen that in the literature, various approaches have been used, comprising various sample preparation techniques, cellulose loadings, and resin compositions. Our approach is able to

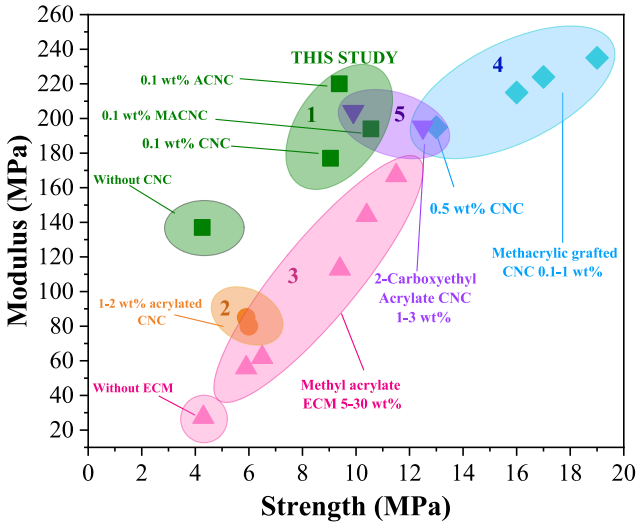

Fig. 8. Ashby plot showing the comparison of tensile tests of composites with added modified cellulose fillers from this work and the literature. (1) our work AESO/ACNC and AESO/MACNC, (2) AESO/acrylate functionalized CNC 1–2 wt % (films) [13], (3) AESO/MA functionalized ethyl cellulose macromonomer (ECM) 5–30 wt% (3D print) [28], (4) methacrylic/MA grafted CNC 0.1–1 wt% (3D print) [29], (5) Epoxy/2-Carboxyethyl Acrylate functionalized CNC 1–5 wt % (cured composites) [12].

integrate the ultra-low loading of 0.1 wt% modified CNC with the bio-based resin from AESO and achieve resin parameters suitable for high resolution VP 3D printing. For this study, the preparation of CNCs was optimized using hydrochloric acid to minimize environmental impact, reduce purification steps, and simplify the preparation procedure. The authors acknowledge that the use of highly processed, purified CNCs of smaller size, prepared via sulfuric acid hydrolysis, is reported in the literature to yield optimal performance. Additionally, hemp stalk waste was incorporated into the preparation process to demonstrate the viability of this alternative.

4. Conclusions

The comprehensive analysis conducted on 3D-printed vegetable oil-based composites filled with neat and modified cellulose nanocrystals (CNC) at a fixed loading of 0.1 wt% is presented in this paper. Utilizing FTIR spectroscopy, we identified distinct functional groups indicative of successful chemical modifications. In addition, filler-matrix interaction analysis revealed the presence of hydrogen and other non-covalent bonding, which significantly affected the material properties. Furthermore, the thermal stability curves of CNC fillers exhibited noticeable changes alongside morphological alterations, providing further evidence of successful modification. Surface wetting studies revealed a considerable shift in the hydrophilicity of the nanocellulose; the contact angle increased from 0° up to 80°, indicating that modified CNCs are more compatible with the matrix. Notably, the addition of CNC fillers to the resin matrix resulted in composites with great printability, as indicated by a smooth surface finish, high transmittance values of up to 80 %, and minimum color changes indicated by colorimetry.

Importantly, our findings demonstrated a significant reinforcement effect on the mechanical characteristics of 3D-printed composites, especially in the modified CNC samples. Tensile and flexural strength improvements of up to 147 % and 121 %, respectively, as well as significant increases in elongation at break up to 75 % (tensile) and 295 % (flexural), demonstrate the effectiveness of the modification procedure. The observed differences in mechanical properties can be related to the modified CNC fillers' unique surface properties, which affect their compatibility and interaction with the polymer matrix. Our findings

revealed a nearly 2-fold increase in crosslink density and a decrease in molecular weight between crosslinks, confirming the impactful influence of CNC fillers in improving the structural integrity of the composite. Dynamic mechanical analysis revealed that CNC fillers increased stiffness and shifted the glass transition region to higher temperatures, resulting in a storage modulus increase of up to 3.4 times in the region above the glass transition. This indicates the remarkable load-bearing capabilities conferred by CNC fillers. The CNC functionalization with methyl methacrylate resulted in slightly superior performance compared to the acrylation approach. Our findings show that modified CNC fillers have a remarkable impact on enhancing mechanical and thermal properties, demonstrating the potential for sustainable resin and its suitability for vat photopolymerization 3D printing.

Funding

A.B. research was funded by Riga Technical University's Doctoral Grant program.

CRediT authorship contribution statement

Beate Beatrise Bruvere: Writing – original draft, Visualization, Validation, Investigation. **Maksims Jurinovs:** Writing – review & editing, Writing – original draft, Visualization, Investigation, Formal analysis. **Oskars Platnieks:** Writing – review & editing, Writing – original draft, Investigation, Formal analysis. **Anda Barkane:** Writing – review & editing, Investigation. **Sergejs Gaidukovs:** Writing – review & editing, Supervision, Resources, Methodology, Conceptualization.

Declaration of competing interest

The authors declare that they have no known competing financial interests or personal relationships that could have appeared to influence the work reported in this paper.

Data availability

Data will be made available on request.

Acknowledgments

The authors wish to thank their parental institute for providing the necessary facilities to accomplish this work.

Appendix A. Supplementary data

Supplementary data to this article can be found online at https://doi.org/10.1016/j.polymer.2024.127453.

References

[1] S. Briede, A. Barkane, M. Jurinovs, V.K. Thakur, S. Gaidukovs, Acrylation of biomass: a review of synthesis process: know-how and future application directions, Curr. Opin. Green Sustainable Chem. 35 (2022) 100626, https://doi.org/10.1016/j.cogsc.2022.100626.

[2] V.S.D. Voet, J. Guit, K. Loos, Sustainable photopolymers in 3D printing: a review on biobased, biodegradable, and recyclable alternatives, Macromol. Rapid Commun. 42 (2021) 2000475, https://doi.org/10.1002/marc.202000475.

[3] V.S.D. Voet, T. Strating, G.H.M. Schnelting, P. Dijkstra, M. Tietema, J. Xu, A.J. J. Woortman, K. Loos, J. Jager, R. Folkersma, Biobased acrylate photocurable resin formulation for stereolithography 3D printing, ACS Omega 3 (2018) 1403–1408, https://doi.org/10.1021/acsomega.7b01648.

[4] R.P. Rosa, G. Rosace, R. Arrigo, G. Malucelli, Preparation and characterization of a fully biobased resin system for 3d-printing, suitable for replacing fossil-based acrylates, J. Polym. Res. 30 (2023) 139, https://doi.org/10.1007/s10965-023-03523-x.

[5] K. Satoh, D.-H. Lee, K. Nagai, M. Kamigaito, Precision synthesis of bio-based acrylic thermoplastic elastomer by RAFT polymerization of itaconic acid derivatives, Macromol. Rapid Commun. 35 (2014) 161–167, https://doi.org/10.1002/marc.201300638.

[6] Z. Karami, M.J. Zohuriaan-Mehr, K. Kabiri, N. Ghasemi Rad, Bio-based thermoset alloys from epoxy acrylate, sesame oil- and castor oil-derived resins: renewable alternatives to vinyl ester and unsaturated polyester resins, Polym. Renew. Resour. 10 (2019) 27, https://doi.org/10.1177/2041247919863633.

[7] J. Thomas, R. Patil, Enabling green manufacture of polymer products via vegetable oil epoxides, Ind. Eng. Chem. Res. 62 (2023) 1725–1735, https://doi.org/10.1021/acs.iecr.2c03867.

[8] A. Babaei-Ghazvini, B. Vafakish, R. Patel, K.J. Falua, M.J. Dunlop, B. Acharya, Cellulose nanocrystals in the development of biodegradable materials: a review on CNC resources, modification, and their hybridization, Int. J. Biol. Macromol. 258 (2024) 128834, https://doi.org/10.1016/j.ijbiomac.2023.128834.

[9] N.B. Palaganas, J.O. Palaganas, S.H.Z. Doroteo, J.C. Millare, Covalently functionalized cellulose nanocrystal-reinforced photocurable thermosetting elastomer for 3D printing application, Addit. Manuf. 61 (2023) 103295, https://doi.org/10.1016/j.addma.2022.103295.

[10] A. Barkane, E. Kampe, S. Gaidukovs, New reinforcing approach for biobased UV-curing resins: hybrid lignocellulose fillers with improved synergy and wood structure mimics, ACS Sustain. Chem. Eng. 11 (2023) 6578–6581, https://doi.org/10.1021/acssuschemeng.2c07288.

[11] E.M. Dogan-Guner, G.T. Schueneman, M.L. Shofner, J. Carson Meredith, Acryloyl-modified cellulose nanocrystals: effects of substitution on crystallinity and copolymerization with acrylic monomers, Cellulose 28 (2021) 10875–10889, https://doi.org/10.1007/s10570-021-04219-5.

[12] A. Ali, T. Aziz, J. Zheng, F. Hong, M.F. Awad, S. Manan, F. Haq, A. Ullah, M. Naeem Shah, Q. Javed, A. Ali Kubar, L. Guo, Modification of cellulose nanocrystals with 2-carboxyethyl acrylate in the presence of epoxy resin for enhancing its adhesive properties, Front. Bioeng. Biotechnol. 9 (2022), https://doi.org/10.3389/fbioe.2021.797672.

[13] N. Auclair, A. Kaboorani, B. Riedl, V. Landry, O. Hosseinaei, S. Wang, Influence of modified cellulose nanocrystals (CNC) on performance of bionanocomposite coatings, Prog. Org. Coating 123 (2018) 27–34, https://doi.org/10.1016/j.porgcoat.2018.05.027.

[14] Y.Q. Qian, N. Han, Y.W. Bo, L.L. Tan, L.F. Zhang, X.X. Zhang, Homogeneous synthesis of cellulose acrylate-g-poly (n-alkyl acrylate) solid-solid phase change materials via free radical polymerization, Carbohydr. Polym. 193 (2018) 129–136, https://doi.org/10.1016/j.carbpol.2018.03.057.

[15] S. Spinella, C. Samuel, J.-M. Raquez, S.A. McCallum, R. Gross, P. Dubois, Green and efficient synthesis of dispersible cellulose nanocrystals in biobased polyesters for engineering applications, ACS Sustain. Chem. Eng. 4 (2016) 2517–2527, https://doi.org/10.1021/acssuschemeng.5b01611.

[16] A. Barkane, O. Platnieks, M. Jurinovs, S. Gaidukovs, Thermal stability of UV-cured vegetable oil epoxidized acrylate-based polymer system for 3D printing application, Polym. Degrad. Stabil. 181 (2020) 109347, https://doi.org/10.1016/j.polymdegradstab.2020.109347.

[17] N. Abidi, L. Cabrales, C.H. Haigler, Changes in the cell wall and cellulose content of developing cotton fibers investigated by FTIR spectroscopy, Carbohydr. Polym. 100 (2014) 9–16, https://doi.org/10.1016/j.carbpol.2013.01.074.

[18] A.R. Fareghi, P.N. Moghadam, J. Khalafy, M. Bahram, M. Moghtader, Preparation of a new molecularly imprinted polymer based on self-crosslinkable cellulose acrylate in aqueous solution: a drug delivery system for furosemide, J. Appl. Polym. Sci. 134 (2017), https://doi.org/10.1002/app.45581.

[19] A. Cogulet, P. Blanchet, V. Landry, Wood degradation under UV irradiation: a lignin characterization, J. Photochem. Photobiol. B Biol. 158 (2016) 184–191, https://doi.org/10.1016/j.jphotobiol.2016.02.030.

[20] R. Rana, R. Langenfeld-Heyser, R. Finkeldey, A. Polle, FTIR spectroscopy, chemical and histochemical characterisation of wood and lignin of five tropical timber wood species of the family of Dipterocarpaceae, Wood Sci. Technol. 44 (2010) 225–242, https://doi.org/10.1007/s00226-009-0281-2.

[21] J.D. Peterson, S. Vyazovkin, C.A. Wight, Kinetic study of stabilizing effect of oxygen on thermal degradation of poly(methyl methacrylate), J. Phys. Chem. B 103 (1999) 8087–8092, https://doi.org/10.1021/jp991582d.

[22] J. Zhang, M.-C. Li, X. Zhang, S. Ren, L. Dong, S. Lee, T. Lei, Q. Wu, Surface modified cellulose nanocrystals for tailoring interfacial miscibility and microphase separation of polymer nanocomposites, Cellulose 26 (2019) 4301–4312, https://doi.org/10.1007/s10570-019-02379-z.

[23] W. Mokrzycki, M. Tatol, Color difference delta E-A survey, mach, Graph. Vis. 20 (2011) 383–411.

[24] ViewSonic, Delta E ≦2 color accuracy. https://www.viewsonic.com/colorpro/articles/detail/deltae2color-accuracy_3. (Accessed 14 November 2023).

[25] A. Kaboorani, N. Auclair, B. Riedl, V. Landry, Physical and morphological properties of UV-cured cellulose nanocrystal (CNC) based nanocomposite coatings for wood furniture, Prog. Org. Coating 93 (2016) 17–22, https://doi.org/10.1016/j.porgcoat.2015.12.009.

[26] M. Jurinovs, A. Barkane, O. Platnieks, S. Beluns, L. Grase, R. Dieden, M. Starpoli, D. F. Schmidt, S. Gaidukovs, Vat photopolymerization of nanocellulose-reinforced vegetable oil-based resins: synergy in morphology and functionalization, ACS Appl. Polym. Mater. 5 (2023) 3104–3118, https://doi.org/10.1021/acsapm.3c00245.

[27] M. Korčušková, V. Sevriugina, F. Ondreáš, J. Svatík, W. Tomal, V. Vishakha, J. Ortyl, P. Lepcio, Photoactivity, conversion kinetics, nanoreinforcement, post-curing, and electric/dielectric properties of functional 3D printable photopolymer resin filled with bare and alumina-doped ZnO nanoparticles, Polym. Test. 116 (2022) 107798, https://doi.org/10.1016/j.polymertesting.2022.107798.

[28] Z. Liu, D.A. Knetzer, J. Wang, F. Chu, C. Lu, P.D. Calvert, 3D printing acrylated epoxidized soybean oil reinforced with functionalized cellulose by UV curing, J. Appl. Polym. Sci. 139 (2022) 51561, https://doi.org/10.1002/app.51561.
[29] B. Wang, J. Liu, K. Chen, Y. Wang, Z. Shao, Three-dimensional printing of methacrylic grafted cellulose nanocrystal-reinforced nanocomposites with improved properties, Polym. Eng. Sci. 60 (2020) 782–792, https://doi.org/10.1002/pen.25336.
[30] S. Beck-Candanedo, M. Roman, D.G. Gray, Effect of reaction conditions on the properties and behavior of wood cellulose nanocrystal suspensions, Biomacromolecules 6 (2) (2005) 1048–1054, https://doi.org/10.1021/bm049300p.